ChemComm

COMMUNICATION

View Article Online
View Journal | View Issue

Cite this: *Chem. Commun.*, 2023, **59**, 9211

Received 1st March 2023,
Accepted 26th June 2023

DOI: 10.1039/d3cc01032e

rsc.li/chemcomm

On the nucleation and fast reaction kinetics of 2D polymerisation with a 2-in-1 monomer†

Niklas Herrmann, [a] Cristina Martin, [b] Samuel Eyley, [c] Yusen Li, [d] Nerea Bilbao,[a] Víctor Rubio-Giménez, [e] Mark Van der Auweraer,[a] Wim Thielemans, [c] Long Chen, *[d] Kunal S. Mali *[a] and Steven De Feyter *[a]

We report on the fast reaction kinetics of an imine based 2D polymer (2DP) formed from a single monomer carrying both aldehyde and amine groups. Our results point towards a direct monomer-to-crystalline polymer transition without an amorphous intermediate.

2D-covalent organic frameworks (2D-COFs) are obtained by covalently linking organic monomers using dynamic covalent chemistry (DCC) which allows harvesting of one desired product out of a combinatorial library under equilibrium conditions. Typically, reversible reactions are employed. The two most widely used reactions are the Schiff base formation[1] and (self)condensation of boronic acids.[2] Boronate ester based 2D-COFs are also popular.[3] 2D-COFs are synthesized using solvothermal methods which employ high temperatures and long reaction times. They are often isolated as crystalline powders which suffer from poor processability.

Another missing piece in the hunt for highly crystalline 2D-COFs is the mechanistic pathway from dissolved molecular monomers to sheets of 2DPs. Despite the wide appreciation of this aspect, the nucleation and growth of synthetic organic 2DPs/2D-COFs remains poorly understood. This is in part due to the relatively harsh reaction conditions used in their synthesis which hinders application of analytical methods for the *in situ* characterisation. Such characterisation is a crucial step in the optimisation of their functional properties.

[a] *Division of Molecular Imaging and Photonics, Department of Chemistry, KU Leuven, Celestijnenlaan 200F, 3001 Leuven, Belgium. E-mail: kunal.mali@kuleuven.be, steven.defeyter@kuleuven.be*
[b] *Department of Physical Chemistry, Faculty of Pharmacy, University of Castilla-La Mancha, Albacete 02071, Spain*
[c] *Sustainable Materials Lab, Department of Chemical Engineering, KU Leuven, Campus Kulak Kortrijk, Etienne Sabbelaan 53, 8500 Kortrijk, Belgium*
[d] *State Key Laboratory of Supramolecular Structure and Materials, College of Chemistry, Jilin University, Changchun 130012, China. E-mail: longchen@jlu.edu.cn*
[e] *Membrane Separations, Adsorption, Catalysis and Spectroscopy, Microbial and Molecular Systems, KU Leuven, 3001 Leuven, Belgium*

† Electronic supplementary information (ESI) available. See DOI: https://doi.org/10.1039/d3cc01032e

Despite the aforementioned challenges, a few studies have already provided important insight into the mechanism of 2D-COF formation.[4–7] One of the early reports pointed towards a two-step mechanism for an imine based 2D-COF, where a quickly formed amorphous intermediate slowly evolves into a crystalline 2D-COF.[4] This mechanism was recently revised suggesting a fast and direct monomer-to-crystalline 2D-COF conversion using transmission electron microscopy (TEM), X-ray diffraction (XRD) and infrared (IR) spectroscopy data.[5] Another study used mass spectrometry to reveal that a self-assembly step precedes the nucleation which yields critical nuclei of covalently linked monomers that then act as seeds for further growth.[6] The insight from mechanistic studies has been used for the successful growth of single crystals of 2D-COFs.[6,7]

The interfacial synthesis of 2DPs is a relatively new synthetic paradigm which allows fabrication of single or few layered films of 2DPs. In this approach, interfaces (solid/gas, solid/liquid, liquid/liquid) are employed as inherently 2D reaction platforms.[8–10] The interfacial polymerisation typically proceeds under relatively mild reaction conditions, and provided that the polymers are fabricated on[3,11] or transferred to[12] atomically flat conductive substrates, allows *in situ* molecular resolution characterisation using scanning tunnelling microscopy (STM).[13]

STM has not only facilitated high-resolution structural characterisation of single layers of 2DPs, but it has also provided detailed insight into the dynamics of 2D polymerisation process.[2] We have recently employed STM for the *in situ* characterisation of nucleation and growth of a boroxine linked 2DP formed at the solution-graphite interface.[14] Both qualitative and quantitative details of the nucleation-elongation processes occurring in real time were obtained. STM data showed an amorphous-to-crystalline transition, time-dependent evolution of nuclei and revealed the existence of non-classical modes of 2D crystallisation and ripening. These findings bode well for further studies for probing mechanistic details of 2D polymerisation processes beyond boroxines.

In this study, we use complementary (surface)analytical techniques, namely, UV-vis spectroscopy, X-ray photoelectron

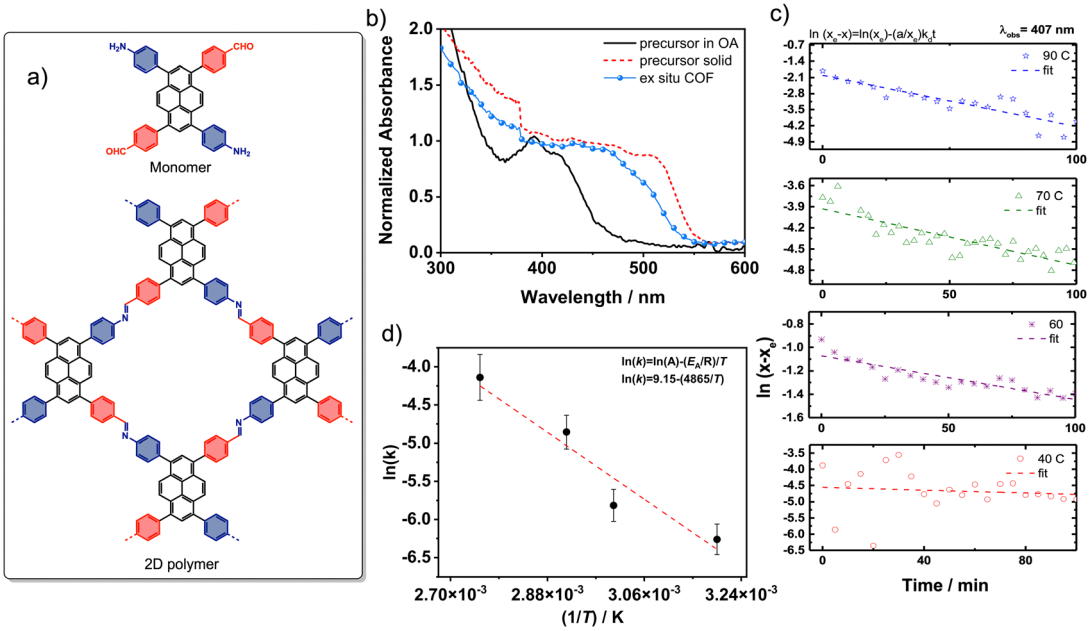

Fig. 1 (a) Chemical structures of the 2-in-1 monomer and the 2D polymer (Py-COF). (b) UV-vis absorption spectrum of the monomer solution in OA/DMSO (black), solid monomer (red), and *ex situ* synthesised Py-COF (blue). In all cases, the absorbance was normalized to one at 390 nm. (c) Determination of the temperature dependent rate constants by recording the evolution of absorbance of the monomer solution (5×10^{-5} M) at 407 nm in OA/DMSO as a function of time. The decrease in absorption is attributed to the formation of Py-COF. The equation for the fitting is a reversible first order reaction $\ln(x_e - x) = \ln\left(\frac{x_0}{x_{0e}}\right) k_D t$, where t, k_d is the direct rate constant and x_0, x_e and x are the concentrations at beginning (t = 0), at the equilibrium (time where k_d = ki) and at a specific time (t) of the reaction. (d) Arrhenius plot for the formation of Py-COF. The slope of the linear-fit model gives the activation energy of the reaction, E_A= 4.5 kJ mol^{-1}.

spectroscopy (XPS), attenuated total reflection infrared spectroscopy (ATR-IR) and STM to study 2D-polymerisation of a so-called 2-in-1 monomer, 4,4′-(3,8-bis(4-aminophenyl)pyrene-1,6-diyl)dibenzaldehyde (Fig. 1a) into the corresponding 2DP. In contrast to typical imine systems which use two different monomers carrying the aldehyde and the amine groups, here a single monomer unit carries both the reactive functional groups with an appropriate substitution pattern. The 2-in-1 monomers have been shown to yield high quality 2D COFs in different solvents under mild conditions.[15,16] Our present experimental results indicate a direct monomer-to-COF pathway without involvement of an amorphous intermediate, following fast nucleation kinetics at room temperature. Furthermore, the results show an in-solution nucleation instead of on-surface nucleation and growth.

The kinetic investigation of the 2D polymerisation of the 2-in-1 monomer was motivated by the fast precipitation of a yellow solid from an octanoic acid (OA) (min. 95%)/dimethyl sulfoxide (DMSO) (max. 5%)/solution of the monomer. In contrast to boronic acid monomers and other bimolecular aldehyde/amine precursor solutions which can be stored in OA/DMSO over weeks at room temperature (RT), the rapid precipitation of the 2-in-1 monomer hinted to a low activation energy compatible with RT synthesis. To gain insight into the kinetics of this reaction, UV-vis absorption spectroscopy was used. Fig. 1b shows the comparison of the UV-vis spectra of the solid monomer, monomer in solution and the solid Py-COF sample. When comparing the spectra, one should note that the spectrum of the monomer in solution is an absorption spectrum of 5×10^{-6} M solution while the spectra of the *ex situ* COF and the solid monomer are reflectance spectra of the solid material.

The spectra of the solid monomer and the *ex situ* COF resemble those reported earlier.[16] They are both strongly red shifted compared to that of the dilute precursor solution. This is probably due to π–π stacking and the resulting exciton interaction.[18] The small blue shift between the solid precursor and the COF can be due to imine bond formation which decreases the electron accepting strength of the carbonyl and the electron donating properties of the amino moiety. This decreased charge transfer (CT) interaction can lead to a blue shift due to the decreased cross conjugation over the pyrene moiety.[17] Although also an alteration of the π–π stacking and the resulting exciton interaction cannot be excluded. While it is difficult to compare the spectra of the dilute solution and solid samples of the precursor of *ex situ* COF information in an absolute way, the kinetics can be obtained by following the evolution of the absorption spectra as a function of time.

By following the decrease of the 407 nm absorption band at temperatures between 25 °C and 90 °C (Fig. 1c) with a fixed monomer starting concentration of 5×10^{-6} M in OA/DMSO (with < 5% V : V DMSO), reaction rate constants were extracted by applying a reversible first order reaction model (full spectra and kinetic fits at all temperatures are shown in the Fig. S1 in the ESI†) by fitting the absorbance as function of time to

$\ln(x_e - x = \ln(x_0/x_{0e})\, k_D t$. The rate constants, k_d, were extracted as 3.2×10^{-5} s^{-1} at 40 °C, 1.3×10^{-4} s^{-1} at 70 °C, and 2.7×10^{-4} s^{-1} at 90 °C (Fig. 1c). Rate constants for bimolecular imine COF system studied by Dichtel *et al.* are one order of magnitude higher (3.5×10^{-3} s^{-1} at 70 °C).[7] We note that these systems differ in solvent composition and the nature of the catalyst.

While the fitting to a first order reversible kinetic pathway models agrees better with the data than a second order fit, we cannot exclude more complex pathways. The imine formation reaction shows an Arrhenius behaviour in this temperature range, with an activation energy of 4.5 kJ mol^{-1} (Fig. 1d). This is in good agreement with experimental and theoretical calculations for the acid-catalysed imine formation with water molecules substantially lowering the activation barriers to values ranging for 8 to 42 kJ mol^{-1}.[19] Here, OA also acts as a protic Brønsted acid catalyst.[16]

Interestingly, the values of the activation energy are lower than those reported for bimolecular boronate ester 2D-COF formation (92–113 kJ mol^{-1}).[18] The appearance of precipitate at RT after 1 h further indicates faster reaction times compared to the boronate ester system (visible solid after 1 h only at 60 °C). This difference can be attributed to the higher probability of two monomer molecules coming together in the right geometry to form an imine bond. Furthermore, the imine formation is catalysed by the presence of an acid and no competing pathway is present (such as the boroxine trimer formation which is possible for the boronic acid precursor).

As the conditions used to study the reaction kinetics differ significantly from those used previously,[16] the product obtained from the OA/DMSO mixture was characterised and compared to the published one.[15] To record the absorption spectrum of the pure (bulk) 2D-COF, the monomer was dissolved in a 1 : 1 (V : V) mixture of OA and DMSO (9×10^{-4} M) and heated to 90 °C for 2 h. Within 10 minutes, a thick yellow precipitate formed. After washing with methanol and drying, a yellow powder, insoluble in all common solvents, was obtained (see details in the ESI†). The UV-vis absorption spectrum of this powder (Fig. 1b) and its ATR-IR spectrum (Fig. 2a) match the reported spectra of the solvothermally synthesised Py-COF solid.[15]

These results motivated us to study the 2D polymerisation of the 2-in-1 system on a solid surface. After drop casting the OA/DMSO solution ($c = 5 \times 10^{-5}$ M) of the 2-in-1 monomer onto highly oriented pyrolytic graphite (HOPG), XPS was performed after drying the samples. In the *N*1s region both imine (398.7 eV) and amine/ammonium (400.2 eV) species could be detected (Fig. 2b).[19] While the presence of an imine signal proves the formation of covalent bonds between the monomer units, the coexistence of amine moieties can be explained with the limited size of the emerging polymer units. The ratio between unreacted end-groups (amine and aldehyde, Fig. 2d) and imine linkages (Fig. 2c) is larger if the size of the 2DP sheets is small. Furthermore, the presence of unreacted monomers cannot be excluded (see also Fig. S6 in the ESI†). While the XPS characterisation confirms the presence of imine nitrogen within the films, the exact nature of the resulting polymer cannot be determined by XPS. Whether the imine containing structures are amorphous or crystalline was confirmed using STM.

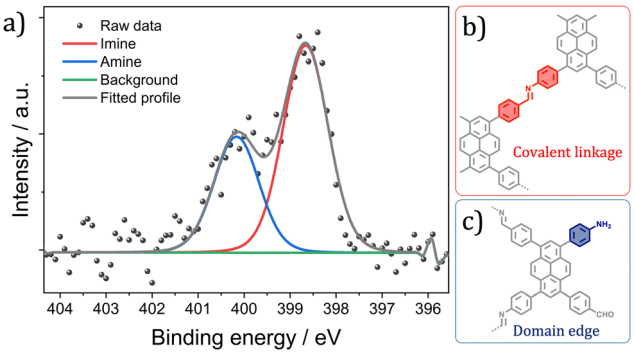

Fig. 2 (a) High-resolution XPS spectrum of a dry thin film of Py-COF deposited on graphite showing the *N*1s region. (b), (c). Chemical schematics showing the possible origin of the imine (c) and the amine (d) nitrogen contribution to the *N*1s signal.

A DMSO stock solution of the monomer was diluted with OA. The resulting slightly yellow solution (5×10^{-5} M) was drop casted onto HOPG at RT and subjected to STM at the solid/liquid interface. Fig. 3a–c show STM images obtained almost immediately after deposition which reveal the formation of small domains of a porous network containing rectangular cavities. The domain size varies between 5 nm to 20 nm. The unit cell parameters obtained from the STM data are $a = 1.6 \pm 0.3$ nm, $b = 1.5 \pm 0.2$ nm, and $\gamma = 90 \pm 3°$ (Fig. 3c). A molecular model presented in Fig. 3d agrees well with the unit cell parameters which in turn are in good agreement with the geometry and unit cell of the bulk Py-COF.[15] The STM data also revealed existence of non-rectangular cavities and multilayers (Fig. S3 in the ESI†).[7] The former could be explained by considering the *E*/*Z* isomerism of the imine bond which could lead to the sporadic formation of isolated six- ($n = 6$) and three-membered ($n = 3$) covalent organic rings co-existing with regular ($n = 4$) COF patches (Fig. S2a and b in the ESI†).

When particles of bulk Py-COF (*vide supra*) were used as seeds for faster nucleation at the liquid-solid interface, reproducibility and the surface coverage was improved. Nevertheless,

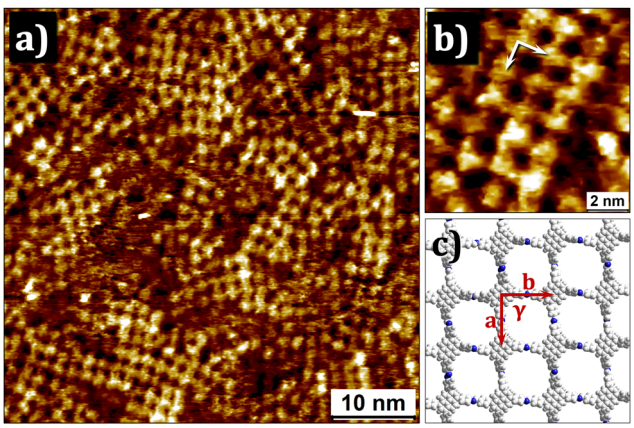

Fig. 3 (a), (b) STM images of 2DP obtained at the liquid/solid interface ($c = 5 \times 10^{-5}$ M in OA/DMSO). (c) Molecular model for the 2DP. Imaging parameters: $V_{bias} = -0.4$ V; $I_{set} = 0.08$ nA.

the overall appearance and the dynamics of the COF flakes on the surface were the same for the seeded and the non-seeded systems. This agrees with single-crystal COFs grown with the seeding approach. While the surface coverage was high and in some cases near total, the size of the COF/nanoflakes did not grow substantially even after prolonged scanning or pulsing (Fig. S4 and S5 in the ESI†). Only the sporadic attachment and removal of single monomers was observed. This is contrary to the boroxine and boronate ester based 2DPs.[20,21] For the latter systems, nucleation was found to occur on the HOPG surface and the subsequent growth and ripening of the domains could be followed over the course of several minutes.[14]

In contrast to the lack of dynamics observed for surface-adsorbed films, the kinetic time series obtained by UV-vis spectroscopy revealed continuous changes in the solution phase even after 1 h (Fig. 1c). This discrepancy between the observations in solution *versus* those made on surface point towards a trapping mechanism, where the deposited 2D COF flakes are removed from the solution equilibrium which in this way shifts to the COF formation. We note that the comparison of kinetic data in-solution and on-surface is not straightforward. Nevertheless, as the nucleation occurs in solution and not on the surface, the pathway from dissolved monomers to the 2D COF nanoflakes seen by STM is not influenced by the presence of the substrate, which only acts as trapping agent stopping the reaction. The limited flake size further explains the amine signal seen in the N1s XPS spectrum (*vide supra*). The surface trapping is absent in solution and thus explains the near complete disappearance of both the carbonyl and amine bands in the IR spectrum of the *ex situ* synthesised bulk COF (Fig. 2a). The residual signal can be either attributed to unreacted monomers or the free end groups of the COF particles. These observations indicate fast nucleation in solution rather than on the HOPG surface. These nuclei, after sufficient growth, are simply deposited on the surface and do not grow further. The existence of multilayers also points towards this hypothesis. The formation of small but crystalline domains with negligible defect density as confirmed from the STM data (Fig. 3a and b) further corroborate that the formation of imine COFs does not occur *via* an amorphous intermediate as previously thought, but directly, through a direct monomer-to-COF mechanism. These observations are further supported by UV-vis study of the system which confirmed the fast nucleation of the 2D polymer in solution. Given the limited time resolution of STM, transient amorphous intermediates (*i.e.*, soluble dimers and trimers) that convert into ordered 2D COF nanoflakes cannot be excluded. Our attempts to compare and contrast the 2D polymerisation behaviour of the 2-in-1 monomer against that of the bimolecular system comprising the corresponding tetraamine and tetraaldehyde did not yield fruitful results, largely due to the extremely low solubility of the tetraaldehyde in common organic solvents (see the ESI†).

In conclusion, we show that a monomolecular 2-in-1 monomer leads to rapid nucleation of a 2D COF in solution under mild reaction conditions at RT. By trapping and imaging the nucleated 2DP flakes on a surface with STM and using UV-vis spectroscopy to analyse the kinetics of the reaction, a direct monomer-to-COF pathway can be deduced for this system, improving our understanding of imine COF formation.

We thank Daniel Hermida Merino for helpful discussions. Financial support through the Marie Skłodowska-Curie project ULTIMATE (GA-813036), Research Foundation–Flanders (FWO) (grant G0A4120N), KU Leuven Internal Funds (grants C14/18/06 and C14/19/079) is acknowledged. We also acknowledge the financial support through grants PID2021-128761OA-C22 funded by MCIN/AEI/10.13039/501100011033, Fondo Europeo de Desarollo Regional (FEDER) by the EU and SBPLY/21/180501/000127 funded by JCCM. N. B. thanks FWO for postdoctoral fellowship (12ZC220N). C. M. thanks financial support *via* grants PID2021-128761OA-C22 funded by MCIN/AEI/10.13039/501100011033 by the "European Union" and SBPLY/21/180501/000127 funded by JCCM and by the EU through "Fondo Europeo de Desarollo Regional" (FEDER).

Conflicts of interest

There are no conflicts to declare.

Notes and references

1 C. Qian, L. Feng, W. L. Teo, J. Liu, W. Zhou, D. Wang and Y. Zhao, *Nat. Rev. Chem.*, 2022, **6**, 881–898.
2 D. Cui, D. F. Perepichka, J. M. MacLeod and F. Rosei, *Chem. Soc. Rev.*, 2020, **49**, 2020–2038.
3 C. Liu, Y. Yu, W. Zhang, Q. Zeng and S. Lei, *Chem. – Eur. J.*, 2016, **22**, 18412–18418.
4 B. J. Smith, A. C. Overholts, N. Hwang and W. R. Dichtel, *Chem. Commun.*, 2016, **52**, 3690–3693.
5 C. Feriante, A. M. Evans, S. Jhulki, I. Castano, M. J. Strauss, S. Barlow, W. R. Dichtel and S. R. Marder, *J. Am. Chem. Soc.*, 2020, **142**, 18637–18644.
6 C. Kang, K. Yang, Z. Zhang, A. K. Usadi, D. C. Calabro, L. S. Baugh, Y. Wang, J. Jiang, X. Zou, Z. Huang and D. Zhao, *Nat. Commun.*, 2022, **13**, 1370.
7 A. M. Evans, L. R. Parent, N. C. Flanders, R. P. Bisbey, E. Vitaku, M. S. Kirschner, R. D. Schaller, L. X. Chen, N. C. Gianneschi and W. R. Dichtel, *Science*, 2018, **361**, 52–57.
8 M. Lackinger, *Polym. Int.*, 2015, **64**, 1073–1078.
9 X. Feng and A. D. Schlüter, *Angew. Chem., Int. Ed.*, 2018, **57**, 13748–13763.
10 X.-H. Liu, C.-Z. Guan, S.-Y. Ding, W. Wang, H.-J. Yan, D. Wang and L.-J. Wan, *J. Am. Chem. Soc.*, 2013, **135**, 10470–10474.
11 Y. Yu, J. Lin, Y. Wang, Q. Zeng and S. Lei, *Chem. Commun.*, 2016, **52**, 6609–6612.
12 D. J. Murray, D. D. Patterson, P. Payamyar, R. Bhola, W. Song, M. Lackinger, A. D. Schlüter and B. T. King, *J. Am. Chem. Soc.*, 2015, **137**, 3450–3453.
13 Y. Hu, N. Goodeal, Y. Chen, A. M. Ganose, R. G. Palgrave, H. Bronstein and M. O. Blunt, *Chem. Commun.*, 2016, **52**, 9941–9944.
14 G. Zhan, Z.-F. Cai, K. Strutyński, L. Yu, N. Herrmann, M. Martínez-Abadía, M. Melle-Franco, A. Mateo-Alonso and S. D. Feyter, *Nature*, 2022, **603**, 835–840.
15 Y. Li, Q. Chen, T. Xu, Z. Xie, J. Liu, X. Yu, S. Ma, T. Qin and L. Chen, *J. Am. Chem. Soc.*, 2019, **141**, 13822–13828.
16 B. Zhang, X. Song, Y. Li, Y. Li, Z. Peng, L. Ye and L. Chen, *Chem. Commun.*, 2020, **56**, 3253–3256.
17 H. Hopf and M. S. Sherburn, *Angew. Chem., Int. Ed.*, 2012, **51**, 2298–2338.
18 B. J. Smith and W. R. Dichtel, *J. Am. Chem. Soc.*, 2014, **136**, 8783–8789.
19 N. Graf, E. Yegen, T. Gross, A. Lippitz, W. Weigel, S. Krakert, A. Terfort and W. E. S. Unger, *Surf. Sci.*, 2009, **603**, 2849–2860.
20 Z.-F. Cai, G. Zhan, L. Daukiya, S. Eyley, W. Thielemans, K. Severin and S. De Feyter, *J. Am. Chem. Soc.*, 2019, **141**, 11404–11408.
21 G. Zhan, Z.-F. Cai, M. Martínez-Abadía, A. Mateo-Alonso and S. De Feyter, *J. Am. Chem. Soc.*, 2020, **142**, 5964–5968.

